Materials Science

Volume 2, Issue 3, 217-229.
DOI: 10.3934/matersci.2015.3.217
Received date 14 May 2015,
Accepted date 03 August 2015,
Published date 11 August 2015

http://www.aimspress.com/

Research article

Coupling (reduced) Graphene Oxide to Mammalian Primary Cortical Neurons *In Vitro*

Antonina M. Monaco [1], Anastasiya Moskalyuk [1], Jaroslaw Motylewski [1], Farnoosh Vahidpour [2], Andrew M. H. Ng [3], Kian Ping Loh [4], Milos Nesládek [2], and Michele Giugliano [1,5,*]

[1] Theoretical Neurobiology and Neuroengineering Laboratory, Dept. of Biomedical Sciences, University of Antwerp, Universiteitsplein 1, 2610 Wilrijk, Belgium
[2] Institute for Materials Research, Material Physics Division, Hasselt University, 3590 Diepenbeek, Belgium; IMOMEC associated laboratory, IMEC, Kapeldreef 75, 3001 Leuven, Belgium
[3] Institute of Materials Research and Engineering, Agency for Science, Technology and Research, 3 Research Link, Singapore 117602
[4] Department of Chemistry and Graphene Research Centre, National University of Singapore, 3 Science Drive 3, Singapore 117543
[5] Brain Mind Institute, Swiss Federal Institute of Technology Lausanne, Switzerland; and Dept. Computer Science, University of Sheffield, S1 4DP, UK

* **Correspondence:** Email: michele.giugliano@uantwerpen.be.

Abstract: Neuronal nanoscale interfacing aims at identifying or designing nanostructured smart materials and validating their applications as novel biocompatible scaffolds with active properties for neuronal networks formation, nerve regeneration, and bidirectional biosignal coupling. Among several carbon-based nanomaterials, Graphene recently attracted great interest for biological applications, given its unique mechanical, optical, electronic properties, and its recent technological applications. Here we explore the use of Graphene Oxide (GO) and reduced Graphene Oxide (rGO) as biocompatible culture substrates for primary neuronal networks developing *ex vivo*. We quantitatively studied cytotoxicity and cellular viability as well as single-cell and network-level electrophysiological properties of neurons *in vitro*. Our results confirm previous reports, employing immortalized cell lines or pluripotent stem cells, and extend them to mammalian primary cortical neurons: GO and rGO are biocompatible substrates and do not alter neuronal excitable properties.

Keywords: graphene oxide; neuroengineering; primary neuronal cultures; cellular electrophysiology; cytotoxicity

1. Introduction

Our fundamental understanding of brain (dys)functions is today at a cross-road. While decades of concerted research led to immense progresses in the field, understanding, repairing, or enhancing the brain still represent the greatest challenges in science and engineering. Recently, advances in nanotechnologies paved the way to a potential revolution in Neuroscience, inspiring many investigators and offering novel tools for studying the brain at the nanoscale [1]. Progresses in material science in particular offered novel perspectives for identifying new ways of repairing and interfacing the brain at the cellular and molecular levels. In fact, micro- and nanostructured materials display intriguing geometrical similarities with the (sub)cellular organization of brain, and have been repeatedly considered as a potential new substrate for engineering future neuroprosthetics [2,3] and novel electrodics. Ultimately, the goal is developing micro- and nanosized sensors and actuators, capable of functional interfacing with the biological tissue and with individual nerve cells at mechanical, chemical, and electrical levels. At the same time, interest for overcoming existing limitations of microfabrication technologies and conventional *in vitro* interfacing techniques [4,5], inherently leading to 2-dimensional neuronal networks, increasingly became widespread. Thus, active research started on 3-dimensional scaffolding for the formation of functional neuronal networks [6] and of brain-like layered tissue [7,8].

Along these lines, Graphene [9,10] as well as other Carbon-based nanomaterials such as Carbon nanotubes became extremely interesting for Neuroscientists, who started numerous studies on their exploitation as nanoscale electrodes, hybrid devices, or nanostructured substrates for neuronal growth and regeneration [2,3,11], investing on their unrivalled electrochemical properties [12-19]. Graphene in particular, a 2D monoatomic layer of C atoms arranged in a honeycomb lattice, is the youngest member of Carbon-based nanomaterials family. Its existence has been first reported in 2004 [13], and rapidly attracted huge attention, as proved by the more than 10’000 papers published on this topic.

Existing biological investigations of Graphene Oxide (GO) and reduced Graphene Oxide (rGO) are becoming increasingly common and today they range from drug delivery and gene therapy [20] to biosensors [21], as well as from electrodes for electrical extracellular stimulation of excitable cells [22] to photothermal tumour ablation therapy [23] and tissue scaffolding [24]. In Neuroscience, GO and rGO have been so far considered as substrates for the growth of neurons [25,26] and for the differentiation of stem cells [27,28], as well as employed as 3-dimensional scaffolds for neural stem cells [29]. Furthermore, Graphene has also recently been exploited in the fabrication of transparent neural electrode arrays [30,31] for both *in vivo* and *ex vivo* electrophysiological and neuroimaging applications. As these applications could lead to long-term, or even chronic, Graphene electrodes implants, we feel that investigations of the elementary properties of GO and rGO in terms of cytotoxicity as well as alteration of the electrical phenotype of cells and networks as observed with

other nanostructured materials [2,11], deserves more attention. Particularly the use of primary mammalian neurons instead of pluripotent or immortalised cell lines is of great importance for future preclinical translation studies.

In this brief contribution, we compare the properties of GO and rGO, obtained by spin coating onto conventional glass coverslips, as substrates for neuronal growth, studying their biocompatibility and whether the electrical properties of neurons and networks are altered.

2. Materials and Methods

2.1. GO and rGO substrates preparation and characterization

GO substrates were prepared by spin coating (2000 rpm, 30 s) GO solution (2mg/ml; Graphene Supermarket, USA) over glass coverslips.

Reduction of GO into rGO was carried electrochemically (Autolab Potentiostat, Metrohm, Singapore), upon immersing GO/glass substrates into a Sodium Phosphate buffer solution (pH = 4.5). The substrates were connected to a working electrode, while an Ag/AgCl electrode and a Pt mesh were used as reference and counter electrodes, respectively. Chronoamperometry was used holding GO/glass substrates at −0.9 V for 1 min. Substrates were then rinsed with deionized water and dried on a heater at 100 °C for 2 min. The morphology of GO and rGO flakes was characterised by Scanning Electron Microscopy (Figure 1a–b) (SEM; FEGSEM JSM 7600F, Jeol, USA), while Atomic Force Microscopy (AFM, ICON-PKG, Bruker, USA) was employed to determine the thickness of GO and rGO layers (Figure 1d–e) by characterising the boundary of the GO/rGO layer and the glass, after exposing by localised minimal scratching the underlying glass layer (Figure 1d). Raman spectra of GO and rGO substrates were finally acquired with a spectrometer (excitation wavelength: 488 nm; Jobin Yvon T64000, Horiba, Japan) at backscattering configuration (Figure 1c).

2.2. Culturing of mammalian primary cortical neurons

GO/rGO were employed as substrate for neuronal culturing and compared to control conditions, represented by the use of standard glass coverslips. To ensure microbiological sterility, all GO/rGO and control substrates were first autoclaved, upon high-pressure saturated steam at 121 °C for 30 min (SA-260FA, Sturdy Industrial Co., LTD, Taiwan). All substrates were then coated with Polyethyleneimine (PEI, Sigma-Aldrich, Belgium) [32], by soaking their surface in a 0.1% PEI solution (w/v) overnight, and afterwards rinsed in deionized water and left drying at room temperature, prior to cell seeding. No adequate cell adhesion was ever observed in the lack of PEI treatment (not shown).

Rat primary neuronal cultures were obtained by standard methods and in accordance with national and institutional guidelines on animal experimentation. Briefly, cortices were dissected from newborn (i.e., postnatal day 0) Wistar rats (Charles River, France), sliced, digested in a trypsin solution (0.025%), and then mechanically dissociated, using repeated passage through the tip of a small glass pipette. Prior to seeding, cells were centrifuged and suspended in Modified Essential Medium supplemented with 50μg/mL gentamycin, 2M glucose, 5% horse serum, and 200mM

l-glutamine (Sigma-Aldrich, Belgium). Cells were seeded at a density of ~1000 mm^{-2}, ensuring rapid maturation of fully functional neuronal networks *ex vivo* [33].

2.3. Cell viability

To assess GO/rGO substrates biocompatibility in terms of cell adhesion and viability, the Live/Dead Cell double staining assay kit (Sigma-Aldrich, Belgium) was performed in neuronal cultures 9 days *in vitro* (DIVs) after plating. Four coverslips for each of the three conditions (i.e., control, GO and rGO), obtained over two distinct culture preparations, were stained. Digital photos from six distinct fields of view for each sample (Figure 2a–c) were acquired using a fluorescence microscope (BX51, Olympus Life Sciences, Belgium) with green (U-MWIBA3, 460–495 nm) and red (U-MWIGA3, 530–550nm) filters, equipped with a digital camera (DP71, Olympus Life Sciences, Belgium). The CellSens software (Olympus Life Sciences, Belgium) was used for image acquisition. Cells were counted using the Cell Counter plugin of ImageJ 1.47v analysis system [34], and densities of alive cells were computed as the average across 24 different images (Figure 2d–e).

To indirectly quantify cell plasma membrane damage or rupture, and thus evaluate cytotoxicity of GO and rGO, the lactate dehydrogenase (LDH) assay test (Sigma Aldrich, Belgium) was used at 9 DIVs. Cell viability was calculated (Figure 2f) as reported in literature [35,36].

2.4. Cellular electrophysiology

Whole-cell patch-clamp electrophysiological recordings were carried out at 34°C from the soma of neurons, at 9–13 DIVs. Intracellular electrical signals were amplified by an Axon Multiclamp 700B Amplifier (Molecular Devices, USA), under voltage- or current-clamp, controlled by the LCG software [37]. Patch pipettes were pulled from standard borosilicate glass (1B150F-4, World Precision Instruments, USA) and filled with solution containing (in mM): 135 K-gluconate, 4 NaCl, 10 HEPES, 10 PC-Na_2, 0.2 EGTA, 4 ATP-Mg^{2+}, and 0.3 GTP-Na_2; pH 7.3 titrated with KOH, resulting in an electrical impedance of 6–8 MΩ. The extracellular solution contained (in mM): 145 NaCl, 4 KCl, 2 Na-pyruvate, 5 Hepes, 5 glucose, 2 $CaCl_2$, and 1 $MgCl_2$; pH adjusted to 7.4 with NaOH. In order to assess passive and excitable electrical properties of single neurons, *ad hoc* current stimulation step-waveforms were injected to estimate the effective membrane time constant and the apparent input resistance (Figure 3a–d). Estimates of the resting membrane potential, as well as the spontaneous emission of action potential were obtained without injecting any stimulus (Figure 4). All recordings were analysed using custom MATLAB scripts (The Mathworks, Natik, USA).

2.5. Statistical analysis

The normality of each data set was tested by the Lilliefors test and subsequent statistical analysis was performed accordingly. For non-normal distributions, Wilcoxon rank sum test was used, while Student's t-test was employed otherwise. Statistical significance has been reported in the figures as $p < 0.05$ (*), $p < 0.005$ (**), and $p < 0.0005$ (***). Data are presented as percentage ±

ratio error, as mean ± standard error of the mean (SEM) for normal distributions, and as median and interquartile range otherwise.

3. Results and Discussion

3.1. Characterization of the rGO/GO substrates

Substrates were characterized using Scanning Electron Microscopy (SEM, Figure 1a–b), Atomic Force Microscopy (AFM, Figure 1d–e), and Raman spectroscopy (Figure 1c). SEM revealed an excellent coverage of GO and rGO flakes, over the entire surface of the glass substrates (Figure 1a–b).

The Raman spectra of GO and rGO samples reveal two of dominant peaks, D and G, present in Graphene [38–40], centered at 1361 and 1603 cm^{-1} for GO, and at 1351 and 1575 cm^{-1} for rGO (Figure 1c). As expected, the ratio of the amplitude of those peaks increases, confirming the successful GO reduction [41,42].

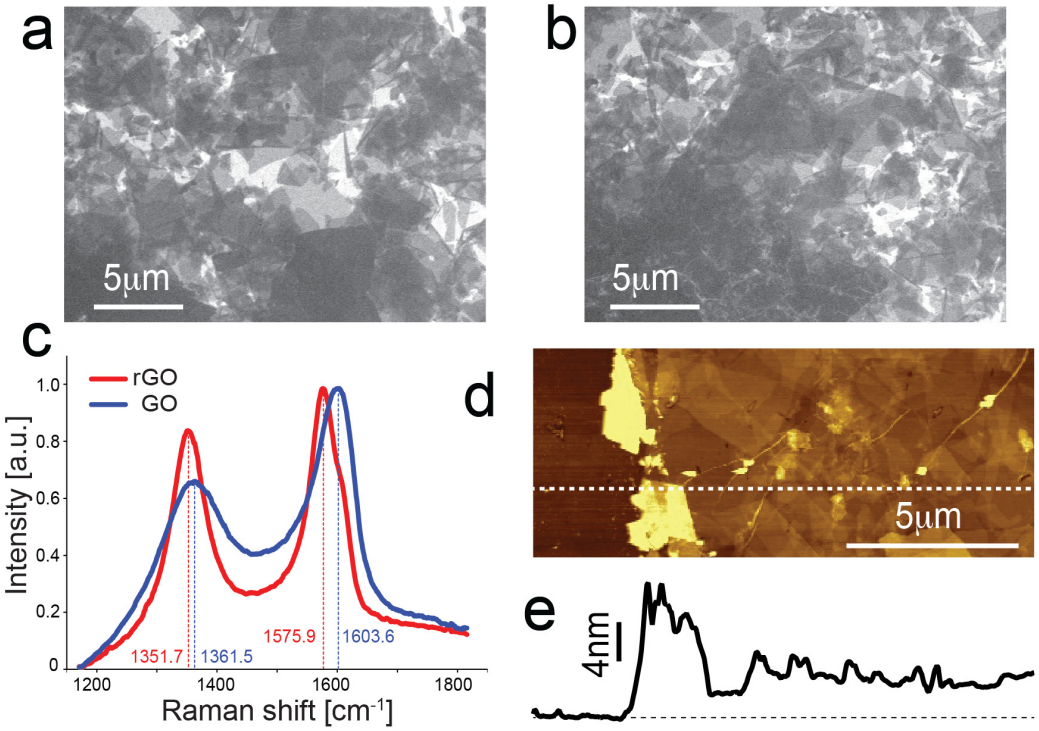

Figure 1. Characterization of the rGO/GO substrates. Images of GO (a) and rGO (b) spin-coated on glass, obtained by scanning electron microscopy with a 5000 times magnification, reveal an even distribution of the flakes on the entire glass substrate. Spectra of rGO/GO (c) show peaks at characteristic Raman shifts typical of Graphene, while Atomic Force Microscopy shows a 4 nm high step profile (e) at the boundary between rGO/GO and the underlying glass substrate, exposed upon scratching (d).

The height profile of deposited Graphene was obtained by AFM at the boundary between rGO/GO and the underlying glass, and revealed a 4 nm thick layer for both samples, with a root mean square value of 2.4 nm (Figure 1d–e).

3.2. Cell viability

A standard assay for cell viability, based on bath application of calcein AM and ethidium homodimer-1 solutions and their read out by epifluorescence, was employed to perform a quantitative analysis of cell viability upon measurements of (live) cell density (Figure 2a–c). The quantification of microscopy images revealed as expected that the total cell density after 9 DIVs decreased to ~50% of the initial seeding density, for both control and rGO. However, the cell density decreased to ~35% of the initial seeding density, for GO substrates (Figure 2d). Interestingly however, the percentage of living cells of out the total calculated for each condition was not significantly different across the conditions, including GO and rGO. Although GO substrates are atomically rougher than rGO [43,44] and thus in principle more likely to promote neuronal adhesion, its superficial charge is known to be more negative than rGO [45,46]. We speculate that the last property might have been then predominant, under our culture conditions, and determining a lower cell adhesion performance in GO compared to rGO and control conditions [47].

We also assessed cytotoxicity of GO and rGO by the lactate dehydrogenase assay (LDH, Sigma Aldrich, Belgium) and observed generally higher membrane damage for neurons grown on GO and rGO, with respect to control conditions (Figure 2f). While this is partly at odd with the clear results of overall cell viability and cellular electrophysiology (Figure 3–4), incongruity might be attributed to suboptimal properties of the Graphene surface coating, prior to cell seeding (i.e., by PEI), or to incompatibility of the LDH assay with the Graphene substrate.

3.3. Cellular Electrophysiology

To investigate the electrical phenotype of neuronal cells growing and establishing functional neuronal networks on GO and rGO substrates, patch-clamp recordings were performed. Live neurons, identified under differential interference contrast videomicroscopy by their morphology and their ability to respond with a sustained train of action potential upon external electrical stimulation, were recorded in whole-cell configuration, after establishing a giga-ohm seal from the cell somata. A variety of current-clamp stimulation waveforms were injected somatically, in order to infer the passive and excitable electrical properties of neuronal membranes (Figure 3). These were the membrane time constant (τ, Figure 3a), the apparent input resistance (R, Figure 3b), the resting membrane potential (E, Figure 3c), the cell capacitance (C, Figure 3d), the width of action potentials (APs) at half-amplitude (Δ, Figure 3e–d), the peak AP amplitude (Figure 3g), the AP threshold (Figure 3h), and the rate of AP emission evoked by external DC current pulses (Figure 3i). Passive properties (R, E, C, τ) did not significantly differed for neurons grown on GO and rGO, compared to control conditions, and also active membrane properties were comparable, with the exception of the peak AP amplitude that was slightly, but significantly larger on GO and rGO, compared to control. Importantly, the functional relationships between the output AP rate and the input injected current

amplitude (Figure 3i) of neurons growing on GO and rGO were undistinguishable, upon removing to each neuron its own rheobase current, for the sake of comparison. Small but significant differences were instead observed solely on the peak AP amplitude (Figure 3e), potentially attributed to marginal heterogeneity of ionic channels expression, (e.g., K_V) whose density and membrane distribution is known to affect AP shape [48].

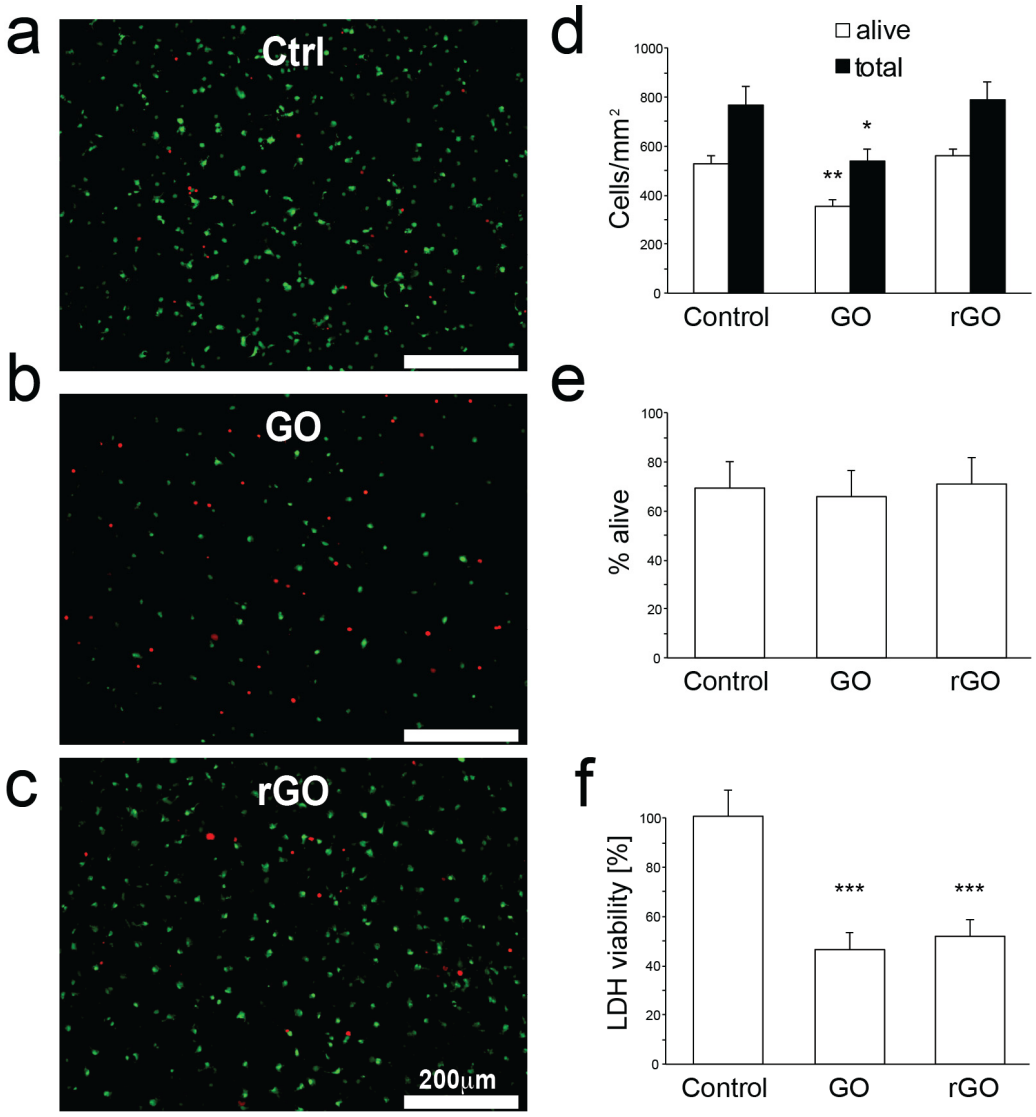

Figure 2. Viability and cytotoxicity of culture substrates. Fluorescence microscopy images (a–c) show living (green) and dead (red) cells. Cell densities (d) and their fraction (e) are quantified by automated cell count and referred to individual substrates. Further cytotoxicity tests revealed potential suboptimal Graphene surface treatment, when compared to control conditions.

The same recording technique, enable us to indirectly infer network properties, by monitoring the spontaneous AP firing rate and frequency of AP burst discharges (Figure 4). When compared to control conditions, neuronal networks formed on GO and rGO had slightly higher spontaneous

activity (Figure 4a–b), significant for GO only, suggesting an earlier formation of synaptic connections or marginally stronger synaptic connectivity than control. Representative intracellular recordings of spontaneous activity are shown in Figure 4c–d.

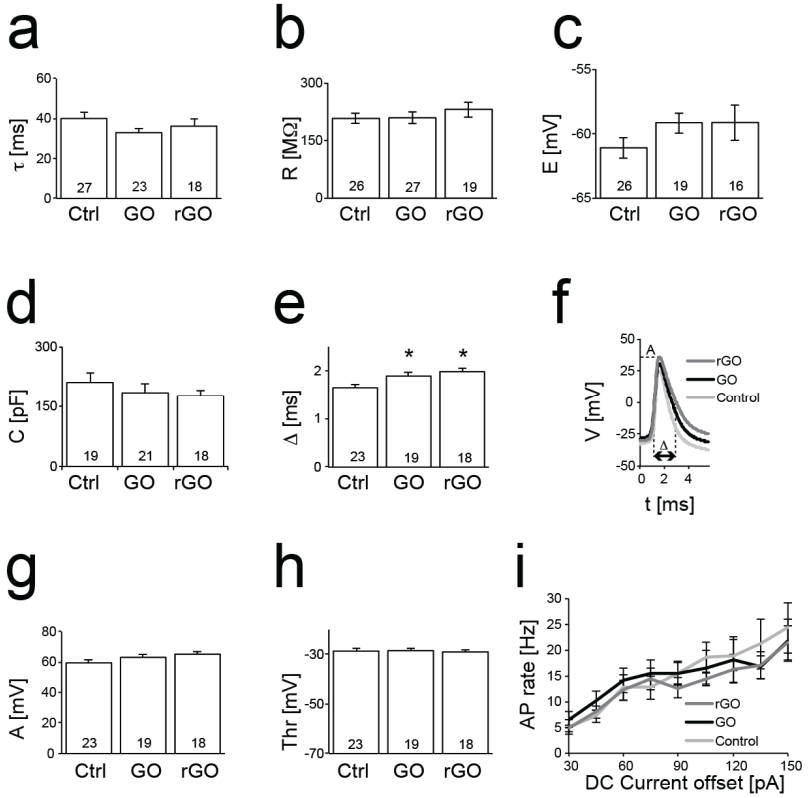

Figure 3. Single-cell passive and excitable electrical phenotype is largely unaffected by the growth substrate. No differences were observed for membrane time constant τ, input resistance R, resting potential E, and membrane capacitance C (a–d). Similarly, active excitable electrical properties (e–h; f, Control: n = 23, GO: n = 19, rGO: n = 18; i, Control: n = 16, GO: n = 14, rGO: n = 16) were unaltered, with the minor yet significant exception of the AP peak amplitude (e). Values inside histograms indicate the number of patched neurons (a–e, g–h).

A corresponding increase in spontaneous postsynaptic currents amplitudes, measured with GO under voltage-clamp conditions, was also observed (not shown).

While distinct network-level electrical phenotype have been reported for neurons coupled to conductive thin-films of carbon nanotubes [11,49], and attributed to specific electrical properties of the substrate [2], GO and rGO seem to largely leave neuronal network formation *ex vivo* unaltered.

Nonetheless, neurons and neural stem cells growing on Graphene [25] and surface-modified GO [47] have increased length and number of neurites [50], which might account for enhanced network connectivity and thus explain the observed increased network activity, despite the reduction in absolute number of neurons. Indeed, number of neurons, efficacy of excitatory synaptic connections or their overall number all influences the rate of spontaneous electrical activity i*n*

vitro [51]. We hypothesize therefore that the slightly increased spontaneous AP firing, observed for neurons grown on GO, is the result of an increased number or efficacy of excitatory synaptic connections rather than a consequence of the absolute number of viable cells. This is supported by the well-known homeostatic scaling of synaptic efficacy [55] and by the variation in the ration of synapses-per-neuron during neuronal maturation [56].

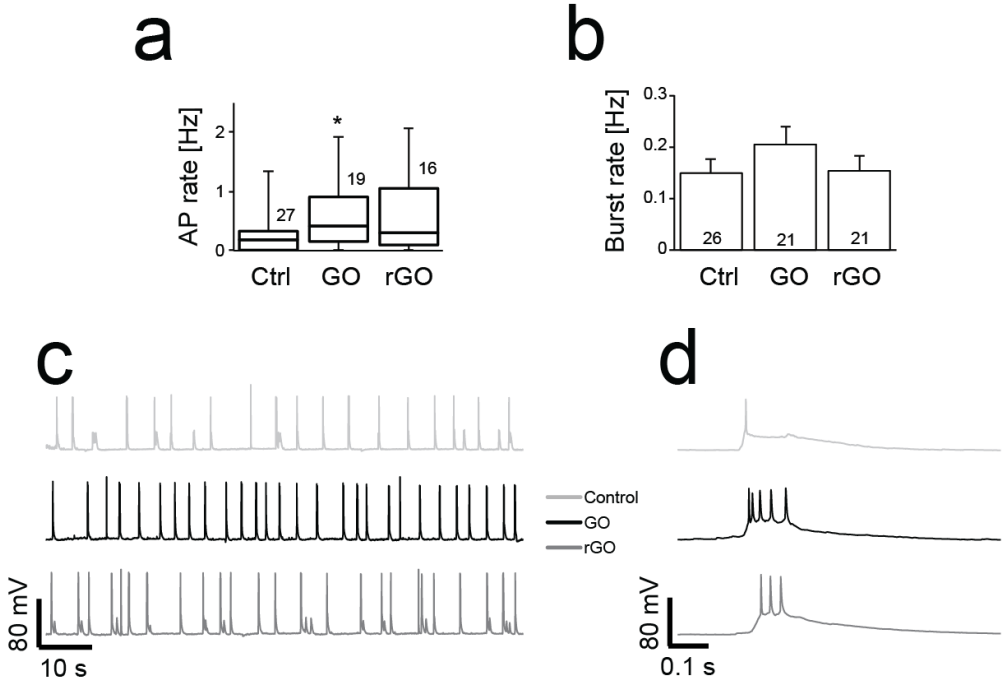

Figure 4. Network-level electrical phenotype is largely unaffected by the growth substrate. No major differences were observed for the rate of spontaneous occurrence of APs (a) and of bursts of APs (b), as also demonstrated by representative raw intracellular voltage recordings (c–d). Values above box-and-whisker plots (a) and inside histograms (b) indicate the number of patched neurons.

On the other side, it has been demonstrated that firing frequency depends on neuronal density [52–54]: very dense cultures or very sparse display lower levels of spontaneous AP firing, than medium dense cultures. Here, we observed generally both a decreased total number of adhered cells and an increased spontaneous activity on GO, confirming the relationship between density and activity, while excluding a direct alteration of network formation by GO.

Similarly, no significant differences were observed also in the rate of occurrence of bursts of APs (Figure 4b), further indicating that recurrent excitatory connections were not altered by GO or rGO [51].

4. Conclusions

In this brief report we presented, to the best of our knowledge, a first quantitative comparison between GO and rGO as substrates for neuronal growth, employing mammalian primary cortical

neurons. We found that GO and rGO are suitable candidates for neuronal interfacing, though rGO displayed better performances than GO, and that both allow the formation of a fully developed and active neuronal network. The electrical phenotype of individual neurons did not appeared altered by the choice of the substrate, while small but significant differences were found in the spontaneous rate of AP firing, greater for neurons grown on GO with respect to both control and rGO conditions.

Acknowledgement

We are grateful to Drs. P. De Marco and G. Panuccio for discussions, and to Mr. D. Van Dyck and M. Wijnants for excellent technical assistance. Financial support from the European Commission (FP7-PEOPLE-IEF "INCA-NANEP", contract n. 328214; FP7-NMP "MERIDIAN", contract n. 280778-02; FP7-"BrainLeap", contract n. 306502), the Flanders Research Foundation (FWO, contract no. G088812N), and the Belgian Science Policy Office (BELSPO) is kindly acknowledged. The funders had no role in study design, data collection and analysis, decision to publish, or preparation of the manuscript.

Contributions

AMM and AM performed electrophysiological experiments, analysed data and wrote the paper. JM performed the viability studies and earlier electrophysiological experiments. FV characterized GO and rGO substrates. AMHN prepared and characterized GO and rGO substrates. LKP, MN, and MG designed and supervised the research. All authors read and approved the final manuscript.

Conflict of Interest

All authors declare no conflict of interest in this paper.

References

1. Alivisatos AP, Andrews AM, Boyden ES, et al. (2013) Nanotools for neuroscience and brain activity mapping. *ACS Nano* 7: 1850–1866.
2. Cellot G, Cilia E, Cipollone S, et al. (2009) Carbon nanotubes might improve neuronal performance by favouring electrical shortcuts. *Nat Nanotechnol* 4: 126–133.
3. Monaco AM, Giugliano M (2014) Carbon-based smart nanomaterials in biomedicine and neuroengineering. *Beilstein J Nanotechnol* 5: 1849–1863.
4. Reinartz S, Biro I, Gal A, et al. (2014) Synaptic dynamics contribute to long-term single neuron response fluctuations. *Front Neural Circuits* 8: 71.
5. Giugliano M, Martinoia S (2006) Substrate Arrays of Microelectrodes forin vitroElectrophysiology.
6. Pautot S, Wyart C, Isacoff EY (2008) Colloid-guided assembly of oriented 3D neuronal networks. *Nat Methods* 5: 735–740.

7. Tang-Schomer MD, White JD, Tien LW, et al. (2014) Bioengineered functional brain-like cortical tissue. *Proc Natl Acad Sci U S A* 111: 13811–13816.
8. Kunze A, Bertsch A, Giugliano M, et al. (2009) Microfluidic hydrogel layers with multiple gradients to stimulate and perfuse three-dimensional neuronal cell cultures. *Procedia Chem* 1: 369–372.
9. Wick P, Louw-Gaume AE, Kucki M, et al. (2014) Classification framework for graphene-based materials. *Angew Chem Int Ed Engl* 53: 7714–7718.
10. Ferrari AC, Bonaccorso F, Fal'ko V, et al. (2015) Science and technology roadmap for graphene, related two-dimensional crystals, and hybrid systems. *Nanoscale* 7: 4598–4810.
11. Mazzatenta A, Giugliano M, Campidelli S, et al. (2007) Interfacing neurons with carbon nanotubes: electrical signal transfer and synaptic stimulation in cultured brain circuits. *J Neurosci* 27: 6931–6936.
12. Falvo MR, Clary GJ, Taylor RM, et al. (1997) Bending and buckling of carbon nanotubes under large strain. *Nature* 389: 582–584.
13. Novoselov KS, Geim AK, Morozov SV, et al. (2004) Electric field effect in atomically thin carbon films. *Science* 306: 666–669.
14. Novoselov KS, Jiang D, Schedin F, et al. (2005) Two-dimensional atomic crystals. *Proc Natl Acad Sci U S A* 102: 10451–10453.
15. Novoselov KS, Jiang Z, Zhang Y, et al. (2007) Room-temperature quantum Hall effect in graphene. *Science* 315: 1379.
16. Katsnelson MI, Novoselov KS, Geim AK (2006) Chiral tunnelling and the Klein paradox in graphene. *Nature Physics* 2: 620–625.
17. Lee C, Wei X, Kysar JW, et al. (2008) Measurement of the elastic properties and intrinsic strength of monolayer graphene. *Science* 321: 385–388.
18. Nair RR, Blake P, Grigorenko AN, et al. (2008) Fine structure constant defines visual transparency of graphene. *Science* 320: 1308.
19. Stoller MD, Park S, Zhu Y, et al. (2008) Graphene-Based Ultracapacitors. *Nano Lett* 8: 3498–3502.
20. Feng L, Zhang S, Liu Z (2011) Graphene based gene transfection. *Nanoscale* 3: 1252–1257.
21. Dey RS, Raj CR (2010) Development of an Amperometric Cholesterol Biosensor Based on Graphene-Pt Nanoparticle Hybrid Material. *J Phys Chem C* 114: 21427–21433.
22. Heo C, Yoo J, Lee S, et al. (2011) The control of neural cell-to-cell interactions through non-contact electrical field stimulation using graphene electrodes. *Biomaterials* 32: 19–27.
23. Yang K, Wan J, Zhang S, et al. (2012) The influence of surface chemistry and size of nanoscale graphene oxide on photothermal therapy of cancer using ultra-low laser power. *Biomaterials* 33: 2206–2214.
24. Kalbacova M, Broz A, Kong J, et al. (2010) Graphene substrates promote adherence of human osteoblasts and mesenchymal stromal cells. *Carbon* 48: 4323–4329.
25. Li N, Zhang X, Song Q, et al. (2011) The promotion of neurite sprouting and outgrowth of mouse hippocampal cells in culture by graphene substrates. *Biomaterials* 32: 9374–9382.
26. Sahni D, Jea A, Mata JA, et al. (2013) Biocompatibility of pristine graphene for neuronal interface. *J Neurosurg Pediatr* 11: 575-583.

27. Nayak TR, Andersen H, Makam VS, et al. (2011) Graphene for controlled and accelerated osteogenic differentiation of human mesenchymal stem cells. *ACS Nano* 5: 4670–4678.
28. Lee WC, Lim CH, Shi H, et al. (2011) Origin of enhanced stem cell growth and differentiation on graphene and graphene oxide. *ACS Nano* 5: 7334–7341.
29. Li N, Zhang Q, Gao S, et al. (2013) Three-dimensional graphene foam as a biocompatible and conductive scaffold for neural stem cells. *Sci Rep* 3: 1604.
30. Kuzum D, Takano H, Shim E, et al. (2014) Transparent and flexible low noise graphene electrodes for simultaneous electrophysiology and neuroimaging. *Nat Commun* 5: 5259.
31. Park DW, Schendel AA, Mikael S, et al. (2014) Graphene-based carbon-layered electrode array technology for neural imaging and optogenetic applications. *Nat Commun* 5: 5258.
32. Ruardij TG, Goedbloed MH, Rutten WL (2000) Adhesion and patterning of cortical neurons on polyethylenimine- and fluorocarbon-coated surfaces. *IEEE Trans Biomed Eng* 47: 1593–1599.
33. Marom S, Shahaf G (2002) Development, learning and memory in large random networks of cortical neurons: lessons beyond anatomy. *Quarterly Reviews of Biophysics* 35.
34. Schneider CA, Rasband WS, Eliceiri KW (2012) NIH Image to ImageJ: 25 years of image analysis. *Nature Methods* 9: 671–675.
35. Aras MA, Hartnett KA, Aizenman E (2008) Assessment of cell viability in primary neuronal cultures. *Curr Protoc Neurosci* Chapter 7: Unit 7 18.
36. Chan FK, Moriwaki K, De Rosa MJ (2013) Detection of necrosis by release of lactate dehydrogenase activity. *Methods Mol Biol* 979: 65–70.
37. Linaro D, Couto J, Giugliano M (2014) Command-line cellular electrophysiology for conventional and real-time closed-loop experiments. *J Neurosci Methods* 230: 5–19.
38. Ferrari AC, Robertson J (2000) Interpretation of Raman spectra of disordered and amorphous carbon. *Physical Review B* 61: 14095–14107.
39. Ferrari AC, Robertson J (2001) Resonant Raman spectroscopy of disordered, amorphous, and diamondlike carbon. *Physical Review B* 64.
40. Ferrari AC (2007) Raman spectroscopy of graphene and graphite: Disorder, electron–phonon coupling, doping and nonadiabatic effects. *Solid State Communications* 143: 47–57.
41. Stankovich S, Dikin DA, Piner RD, et al. (2007) Synthesis of graphene-based nanosheets via chemical reduction of exfoliated graphite oxide. *Carbon* 45: 1558–1565.
42. Cui P, Lee J, Hwang E, et al. (2011) One-pot reduction of graphene oxide at subzero temperatures. *Chem Commun (Camb)* 47: 12370–12372.
43. Andre Mkhoyan K, Contryman AW, Silcox J, et al. (2009) Atomic and electronic structure of graphene-oxide. *Nano Lett* 9: 1058–1063.
44. Paredes JI, Villar-Rodil S, Solis-Fernandez P, et al. (2009) Atomic force and scanning tunneling microscopy imaging of graphene nanosheets derived from graphite oxide. *Langmuir* 25: 5957–5968.
45. Li D, Muller MB, Gilje S, et al. (2008) Processable aqueous dispersions of graphene nanosheets. *Nat Nanotechnol* 3: 101–105.
46. Li M-j, Liu C-m, Xie Y-b, et al. (2014) The evolution of surface charge on graphene oxide during the reduction and its application in electroanalysis. *Carbon* 66: 302–311.

47. Tu Q, Pang L, Chen Y, et al. (2014) Effects of surface charges of graphene oxide on neuronal outgrowth and branching. *Analyst* 139: 105–115.
48. Bean BP (2007) The action potential in mammalian central neurons. *Nat Rev Neurosci* 8: 451–465.
49. Lovat V, Pantarotto D, Lagostena L, et al. (2005) Carbon nanotube substrates boost neuronal electrical signaling. *Nano Lett* 5: 1107–1110.
50. Tang M, Song Q, Li N, et al. (2013) Enhancement of electrical signaling in neural networks on graphene films. *Biomaterials* 34: 6402–6411.
51. Giugliano M, Darbon P, Arsiero M, et al. (2004) Single-neuron discharge properties and network activity in dissociated cultures of neocortex. *J Neurophysiol* 92: 977–996.
52. Biffi E, Regalia G, Menegon A, et al. (2013) The influence of neuronal density and maturation on network activity of hippocampal cell cultures: a methodological study. *PLoS One* 8: e83899.
53. Wagenaar DA, Pine J, Potter SM (2006) An extremely rich repertoire of bursting patterns during the development of cortical cultures. *BMC Neurosci* 7: 11.
54. Cohen E, Ivenshitz M, Amor-Baroukh V, et al. (2008) Determinants of spontaneous activity in networks of cultured hippocampus. *Brain Res* 1235: 21–30.
55. Turrigiano GG, Leslie KR, Desai NS, et al. (1998) Activity-dependent scaling of quantal amplitude in neocortical neurons. *Nature* 391: 892–896.
56. Cullen DK, Gilroy ME, Irons HR, et al. (2010) Synapse-to-neuron ratio is inversely related to neuronal density in mature neuronal cultures. *Brain Res* 1359: 44–55.

AIMS Press